Charles University in Prague

Faculty of Mathematics and Physics

BACHELOR THESIS

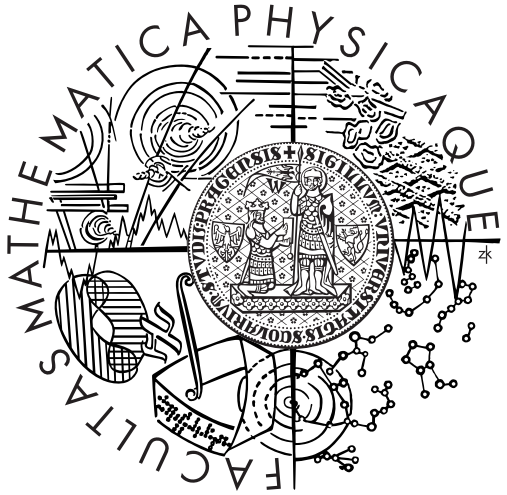

Jozef Koval'

Design of semicondutor detector for the Belle II experiment

Institute of Particle and Nuclear Physics

Supervisor: Peter Kodyš, PhD.

Study programme: General physics

Prague 2011

I would like to take advantage of this situation and thank everyone who supported me during the time I was writing this thesis.

Firstly, I am very grateful to my family for every kind of help they gave me. Even if they are hundreds of kilometers away from me, I can still feel and see their support. Then, of course I want to mention my supervisor, Dr. Peter Kodyš, who was very patient and helpful, everytime I had some problems or troubles. I would also like to express my gratitude to all members of our team, namely to Dr. Peter Kvasnička, Dr. Zdeněk Doležal and Dr. Zbyněk Drásal.

Great thanks belongs to František Glova and to his grammar corrections of the text.

I declare that I carried out this bachelor thesis independently, and only with the cited sources, literature and other professional sources.

I understand that my work relates to the rights and obligations under the Act No. 121/2000 Coll., the Copyright Act, as amended, in particular the fact that the Charles University in Prague has the right to conclude a license agreement on the use of this work as a school work pursuant to Section 60 paragraph 1 of the Copyright Act.

Prague, August 3, 2011

Názov práce: Návrh kremíkového detektoru pre experiment Belle II

Autor: Jozef Kovaľ

Ústav: Ústav částicové a jaderné fyziky

Vedúci bakalárskej práce: RNDr. Peter Kodyš CSc., Ústav částicové a jaderné fyziky

Abstrakt: Predložená bakalárska práca sa zaoberá overením energetických strát a kontrolou implementácie materiálu do softwaru vo vnútornom dráhovom detektore experimentu Belle II v Japonsku. K overeniu bolo použité prostredie basf2, ktoré je vyvýjané špeciálne pre tento experiment.

Prvá časť práce teoreticky popisuje experiment Belle II, jeho vnútorný pixelový kremíkový detektor DEPFET a softwarový simulačný a analytický nástroj basf2 vyvinutý pre Belle II. V druhej časti práce sú zhrnuté poznatky o stratách energie častíc, ktoré prelietavajú materiálom. Posledná časť porovnáva teoretické hodnoty s hodnotami získanými prostredníctvom simulácií v prostredí basf2.

Kľúčové slová: kremíkový detektor, pixelový detector, DEPFET, Belle II, basf2, Geant4, energetické straty

Title: Design of semicondutor detector for the Belle II experiment

Author: Jozef Kovaľ

Department: Institute of Particle and Nuclear Physics

Supervisor: Peter Kodyš, PhD., Institute of Particle and Nuclear Physics

Abstract: This bachelor thesis deals with the verifying of energy losses and checking the implementation of material into software on the inner tracking detector in the Belle II experiment in Japan. The Basf2 framework, which is developed especially for this experiment, was used for this confirmation.

First part of the thesis theoretically describes the Belle II experiment, it's inner pixel silicon detector DEPFET and also describes software and analytics framework - Basf2, which is developed for Belle II. Second part presents the knowledge about the energy losses of the particle passing through matter. The last part compares theoretical values with the values acquired from the basf2 simulation.

Keywords: semiconductor detector, pixel detector, DEPFET, Belle II, basf2, Geant4, energy losses

Contents

Introduction

What we observe is not nature itself, but nature exposed to our method of questioning.

Werner Heisenberg

Human kind has always been interested in the questions which are not easy to understand and accept. In the recent decades, physics has played quite important role in discovering the answers of such a questions. At the end of 19th century, everything in physics was described and only few experiments were waiting to be explained. But these experiments, such as photoelectric effect or Michelson-Morley experiment, opened the door of physics to the two new great "fields", relativity (special and later general) and quantum theory (mechanics, electrodynamics and chromodynamics). It can be safetly said that the beginning of 20th century was the biggest physics revolution which has occured in the history of physics.

One of the questions, which has not been answered yet, is about the beginning of our universe. Experiments of astrophysics (great telescopes) can "see" the history of our universe only up to 384 thousands years after the big bang. Particle physics has made a great progress in this field and nowadays we basicly know everything what happened after 10^{-36}s of big bang.

Last experiments have proved the theory which is often called Standard Model (SM). However, in spite of the fact that this theory was published 30 years ago, there is still one piece of Standard Model theory "puzzle" which is missing. Higgs boson(s).

On the other hand, another experiments have discovered strange attributes of particles behaviour which are not able to be explained by SM. There are also questions why Standard Model needs so many free parametres, what determines the mass of the fundamental particles, how can we explain their hierarchy, etc. One of the most interesting problem is the matter-antimatter asymmetry in our universe. We know that CP violation (violation of charge conjugation symmetry - C symmetry and parity symmetry - P symmetry), currently described by Cabibbo-Kobayashi-Maskawa (CKM) matrix is the source of the matter-antimatter assymetry, but CKM is unable to explain it. So it implicates that there must be another mechanism or source of CP violation.

There are several theories which have potential to describe and explain physics "beyond" SM, sometimes called New Physics (NP). These theories predicts, for

instance, existence of supersymmetrical particles with masses of TeV order (supersymmetry theory - SUSY), or existence of some extra dimensions (string theory).

But every theory needs to be proved by experiment. That is the reason why the human kind build accelerators and particle colliders around the world. As it will be discussed in the first chapter, there is also one very succesfull experiment in KEK, Japan, called Belle, which is going to be upgraded to Belle II. In the second chapter the inner pixel vertex detector for this experiment will be described and his advantages will be shown. The third chapter will be aimed on the software framework used for the simulation in this experiment and on the simple explanation of its usage. In the following chapter the theory of energy loss will be discussed and there will be also explained 2 level model which is used in the simulation. The last chapter will compare theoretical results and the results which come from simulation.

Chapter 1

Belle II

1.1 KEK and Belle experiment

The center for high energy accelerator research organization (KEK) in Tsukuba, Japan, has provided experiments at the field of particle physics for a long time. To be short, it is necessary to mention experiments like PS (Proton Synchrotron), PF (Photon Factory), TRISTAN (Transposable Ring Intersecting Storage Accelerator in Nippon), KEKB (KEK B-factory), K2K (Neutrino Oscillation experiment), J-PARC (Japan Proton Accelerator Research Complex). But probably the most famous was Belle experiment. In 2001, two independent groups (BaBar and Belle) discovered broken symmetries and their results leaded to Nobel Prize for Kobayashi, Maskawa and Nambu in 2008. That situation only proved the willing of many scientists to upgrade the Belle experiment. The decision came really soon, in 2008 there was first meeting of Belle II collaboration.

The Belle experiment observed many interesting events to study. The following list is not trying to describe all of them, it just wants to show the importance of Belle experiment for particle physics (see reference [16] for more detailed explanation).

- In 2002 and 2003, mixing-induced time-dependent CP violation (TCPV) of the neutral B mesons was observed. Following decays were analyzed: $B^0 \to J/\psi K^0$ [18], $B^0 \to \pi^+\pi^-$ [19].

- The new resonance $X(3872)$ was discovered in 2003 [25]. Its study by Belle II will help us to better understand quantum chromodynamics.

- Next year, the direct CP violation (DCPV) in B decays was observed [20, 21]

- In 2006 the purely leptonic decay was observed [22] in the following decay $B^+ \to \tau^+\nu_\tau$

- Two years later, data proved that DCPV in $B^+ \to K^+\pi^0$ is different as in $B^0 \to K^+\pi^-$ [26]. The SM is unable to explain it.

1.2 Belle vs. Belle II

According to the fact that Belle II is upgrade of Belle, let us compare the old and the new experiment.

The new detector has basicly, the same structure as old one, with few significant changes. The vertex detector will also contain Pixel Detector (PXD). That means, the vertex resolution is much better due to great spatial resolution of pixel detector. In the barrel and endcap area, there are completly new systems for identifying particles with really fast readout electronics.

Other changes are:

- smaller energy beam assymetry (Belle: 8 GeV/c on 3.5 GeV/c, Belle II: 7 GeV/c on 4 GeV/c)
- Silicon Vertex Detector radius of outermost layer has larger radius
- Central Drift Chamber (CDC) will have smaller drift cells than in Belle
- faster electronics for readout, lower noise occupancy

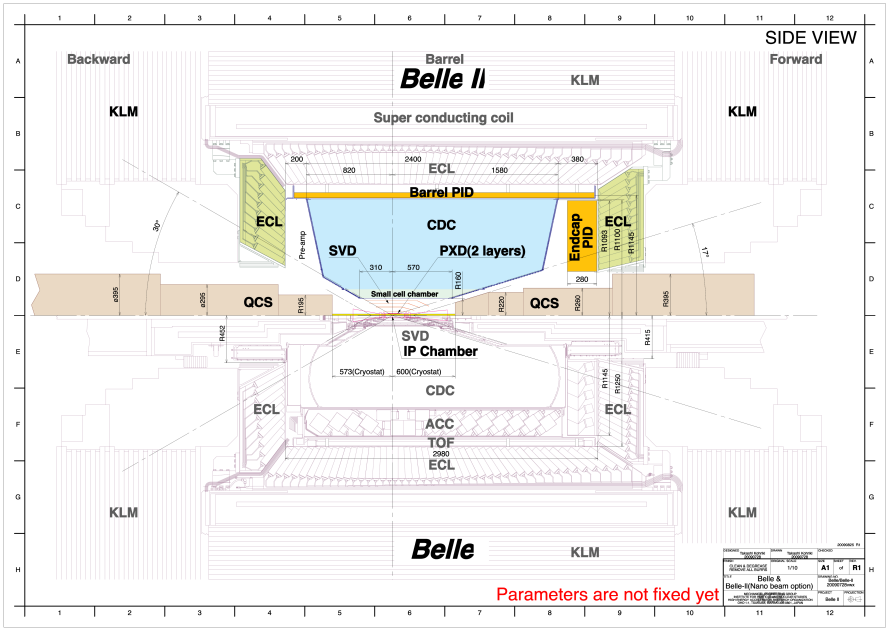

Figure 1.1: The expected geometry of new Belle II detector [16].

1.3 Energy and statistics

As has already been described in the introduction, potential discovers of new physics are expected. You might ask how is that possible if we have energy in order of GeV and we want to study processes which occurs at TeV scale. Let

me answer this question with following example [15]. In the medieval age people looked at the moon and thought what could be there. Someone could say we would not know that until we go there. On the other hand some clever scholar invented telescope so we could actually see and study moon. And long time before Neil Armstrong took the "small step for a man" in 1969, we already knew many of the information about the moon.

The similar story happens in particle physics. We can study and discover many properties of particles and their interactions. Of course we need something like our "telescope". One of the most important factors which we should take care about is statistics. Some of the processes or interactions occurs at the lower energy rate but their probability is very small. If we are able to record many events, there is also higher chance we can find some interesting events.

The following picture shows various approach of different colliders for searching new physics. The LHC and Tevatron look for it directly, but KEKB and SuperKEKB indirectly.

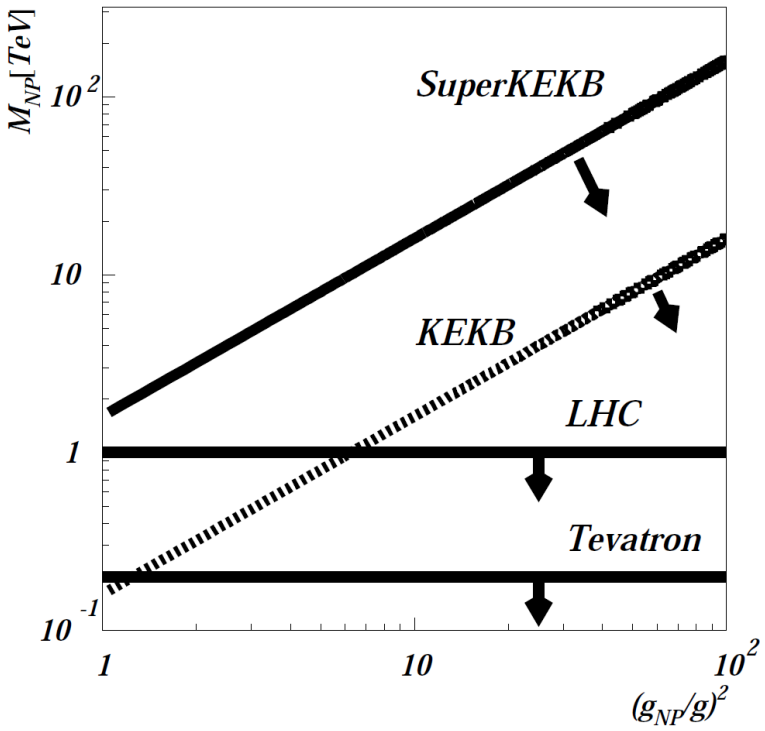

Figure 1.2: Searching for New Physics (NP) and sensitive regions of various colliders. Sensitivity to NP depends on strength of the flavor violating couplings of NP [16].

1.4 Luminosity

As we mentioned in previous section, statistics seems to play very important role in looking for new physics by indirect approach. Statistics in particle physics is closely related to variable $\mathcal{L}$, which is called luminosity and defined as

$$N = \mathcal{L}\ \sigma \tag{1.1}$$

where N is number of recorded events and σ is the total cross section of specific reaction. Usually, luminosity is expressed in units $\mathrm{cm}^{-2}\ \mathrm{s}^{-1}$. Luminosity is influenced by the quality of the beams, which have typical structure. In the case of SuperKEKB it is so called "Nano-Beam" scheme (fig. 1.3). This idea originaly comes from Italy [34].

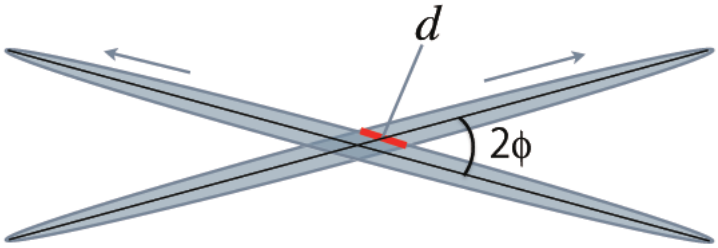

Figure 1.3: Nano-Beam scheme (illustrative picture) [16].

The luminosity is expressed as:

$$\mathcal{L} = \frac{\gamma_{\pm}}{2er_e}\left(\frac{I_{\pm}\xi_{y\pm}}{\beta^*_{y\pm}}\right)\left(\frac{R_L}{R_{\xi_y}}\right) \tag{1.2}$$

where γ is Lorenz factor, e and r_e electric charge and the classical radius of electron, I is total beam current, ξ_y vertical beam-beam parameter, β^*_y vertical beta function at the interaction point. R_L and R_{ξ_y} represents reduction factors for luminosity and vertical beam-beam parameter. Suffix $(-)$ stands for electron, suffix $(+)$ for positron. Figure 1.4 shows specific parameters for KEKB and SuperKEKB.

The characteristic which gives us some information about the effectiveness of the particle collider during some period of time is luminosity integrated through time (also called integrated luminosity), which is usually expressed in units of inverse femtobarns ($1\mathrm{fb}^{-1}$). On November, 29th, KEKB integrated luminosity reached $1000\mathrm{fb}^{-1}$ [35]. The expected value of integrated luminosity for SuperKEKB is $50\mathrm{ab}^{-1}$[16], which is 50 times more than in the old experiment.

	KEKB Achieved	SuperKEKB
Energy (GeV) (LER/HER)	3.5/8.0	4.0/7.0
ξ_y	0.129/0.090	0.090/0.088
β_y^* (mm)	5.9/5.9	0.27/0.41
I (A)	1.64/1.19	3.60/2.62
Luminosity ($10^{34}\mathrm{cm}^{-2}\mathrm{s}^{-1}$)	2.11	80

Figure 1.4: Parameters for KEKB and SuperKEKB factories taken from [16].

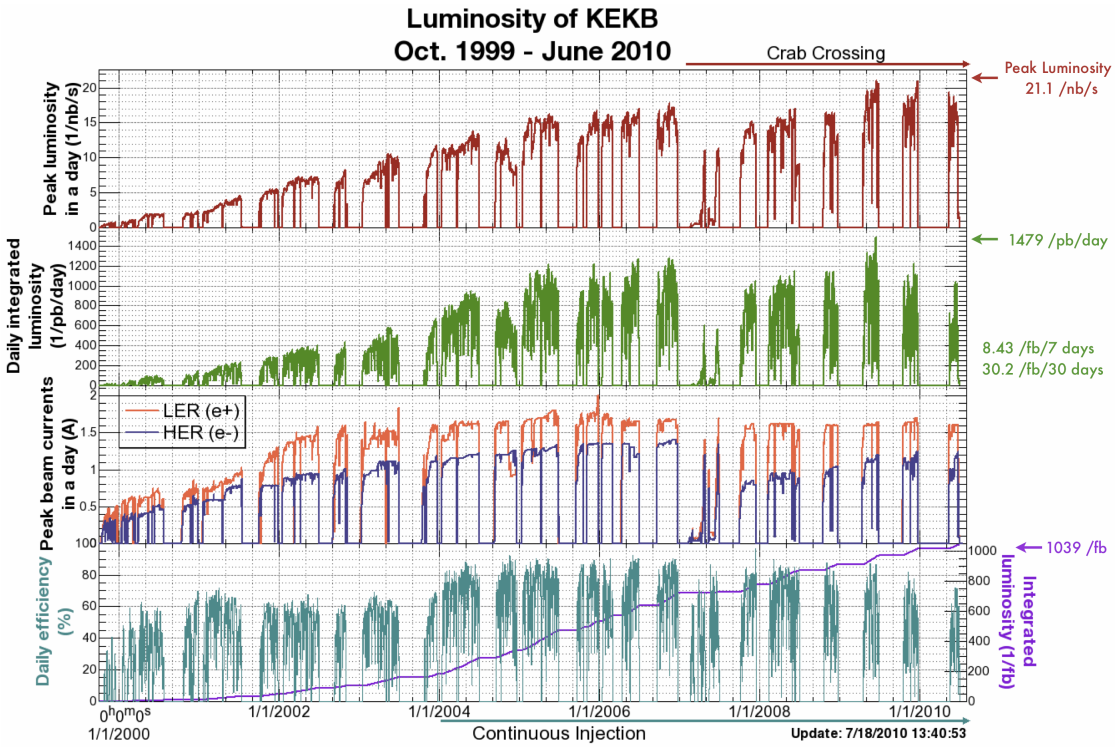

Figure 1.5: Various graphs for KEKB luminosities (peak, integrated, daily) and also beam currents and daily efficiency for overall period of running Belle experiment [33].

Chapter 2

Pixel Detector

The way how we detect particles is through detectors. Every experiment have its own specialized detectors. Basicly, we want as much information as possible about the particles we detect. As we cannot achieve it with single detector, we integrate detetectors into detector systems.

So called tracing detectors determine the trajectory of charged particle. They are placed in the magnetic field so from the track curvature we can determine particles momentum and charge.

In general there are two families of tracking detectors. Gaseous and solid state tracking detectors. General idea of gaseous tracking detector is that particle go through gas and creates electron-ion pairs along its track. Then the electrons drift to the wire and we measure the signal. Examples of gaseous tracking detectors are: ionization chamber, multiwire chamber, spark chamber, proportional chamber, multiwire proportional chamber, drift chamber, time projection chamber, etc.

The greatest family of solid state tracking detectors consist of semiconductor detectors. Many materials are used such as silicon (mostly), diamond, germanium. The idea is the same as with gaseous tracking detectors, but we use solid material instead of gas. The material of detector is highly doped, making it into the diode which is reverse biased. Mostly used semiconductor are: strip detectors (narrow strips are doped), drift detectors, CCD (charge-coupled device), APD (avalanche photodidodes), pixel detectors.

Belle II experiment is heavily interested in the decays of neutral particles such as B, K, D. The neutral particle is not detected by detector, but it often decays into charged particles. The so called "vertexes" (or positions) of this decays are very important for finding new physics. As the experiment needs precise vertex and track measurements, pixel detector is perfect choice. Inner pixel detector is a new feature of the Belle II experiment.

Several monolithic pixel sensors have been designed and realized as prototypes (MPS - Monilithic Pixel Sensors, MAPS - Monolithic Active Pixel Sensors), but only DEPFET (DEPleted Field Effect Transistor) satisfy requirements to design and was ready to be usable in requested time period. Its funding was also secured. This is going to be the first time in the history of particle physics, when the detector system contains monolithic pixel detector.

2.1 Development

The first concept of DEPFET detector was published by Kremer and Lutz in 1987 [29]. Since then this concept has been heavily developed. The DEPFET is a high precision pixel vertex detector, which provides additional tracker hits. These hits improve the overall tracking efficiency and specify positions of vertexes of particle's decays, from which the new physical conclusions can be determined. As the typical vertex detector, DEPFET is placed very close to the interaction point, it is robust against the strong machine-induced background, synchrotron radiation, back scattered photons and neutrons. On the other hand, power consumption is minimized. All these features make DEPFET the ideal candidate as the vertex detector for experiments in particle physics. Except Belle II experiment it should be also used in the brand new electron-positron collider ILC (International Linear Collider).

Except the high energy physics, DEPFET is going to be used in experiments for X-Ray astronomy and also in biomedicine.

2.2 Principle

The principle of DEPFET, which is monolithic detector, is that the first amplified transistor is integrated into a sensor. Sporadical capacitances are annuled because of short connections between sensor and amplifier and very small input capacitance is achieved. This is the reason why DEPFET has such a low-noise performance.

In DEPFET case, a p-channel MOSFET (Metal Oxide Semiconductor Field Effect Transistor) is the first amplifying transistor. The sensor material contains thin, fully depleted, high resistivity silicon substrate.

Whole principle of DEPFET detector works in a following way (Fig. 2.1). There is a potential minimum for electrons created under the transistor channel because of depletion and additional n-implantation below the MOSFET. This can be considered as an internal gate of the MOSFET. The backside of the device has been optimized for low-energy radiation detection. It is composed of a p+ implant and a passivation layer.

Particles which enter the detector, generate electron–hole pairs within the fully depleted bulk. Holes drift into the rear contact of the detector and the electrons are centered in the potential minimum (also called internal gate) where they are stored. Afterwards, signal charge leads to a change in the potential of the internal gate, resulting in a modulation of the channel current of the MOSFET.

The readout can be repeated. The internal gate of the transistor is filled up with signal charges so this charges have to be removed from time to time. This can be managed by applying a positive voltage pulse to an additional n-type contact next to the transistor, also known as the clear contact.

The signal charge is stored in the pixel cell and pixel does not need to be read out persistently. In comparing with other pixel sensor concepts, this can be used to reduce the number of readout channels.

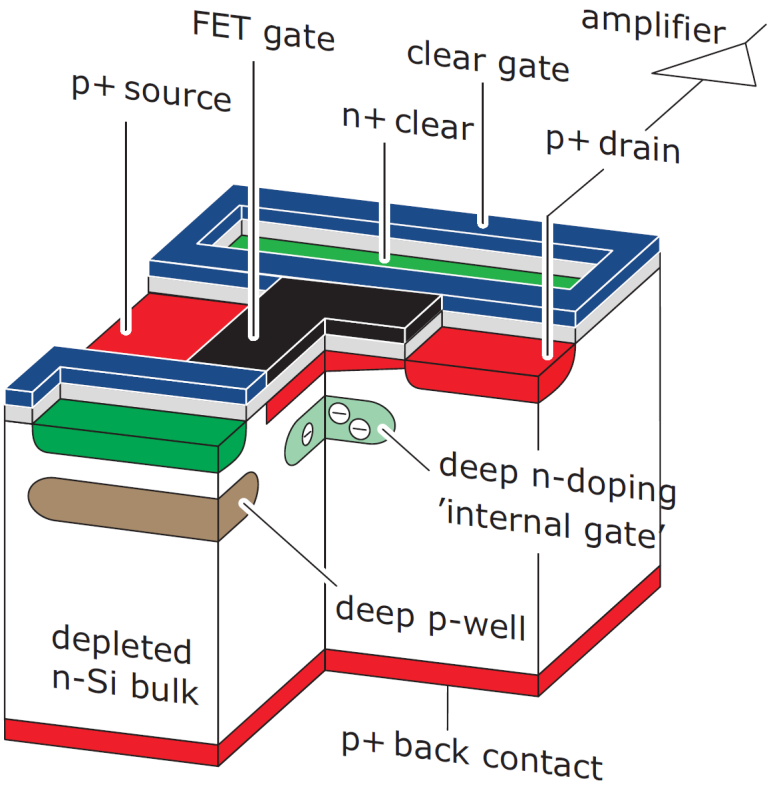

Figure 2.1: Schematic picture of one DEPFET pixel [16].

2.3 Space layout and the structure of PXD

Geometrical layout is based on the system of 2 layers of DEPFET sensors. The innermost layer is located very close to the interaction point. First layer has radius 14mm and second 22mm. Every layer consists of the plain sensors, often called ladders. There are 8 laders in first layer and 12 in the second layer. Every ladder consist of 2 silicon active parts.

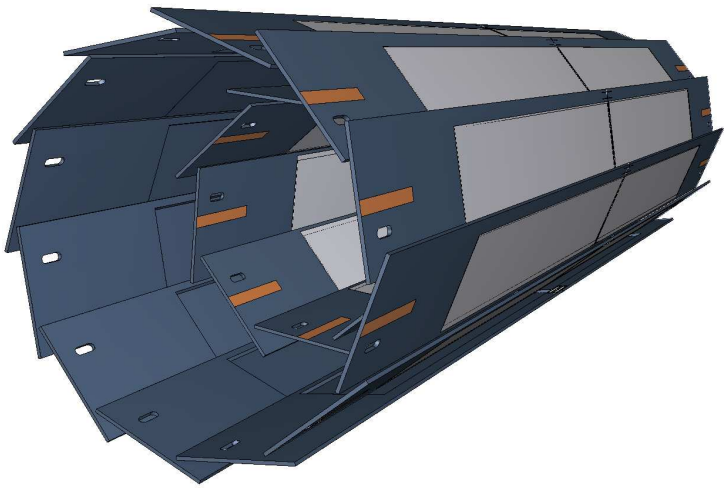

Figure 2.2: Geometrical layout of the DEPFET [16].

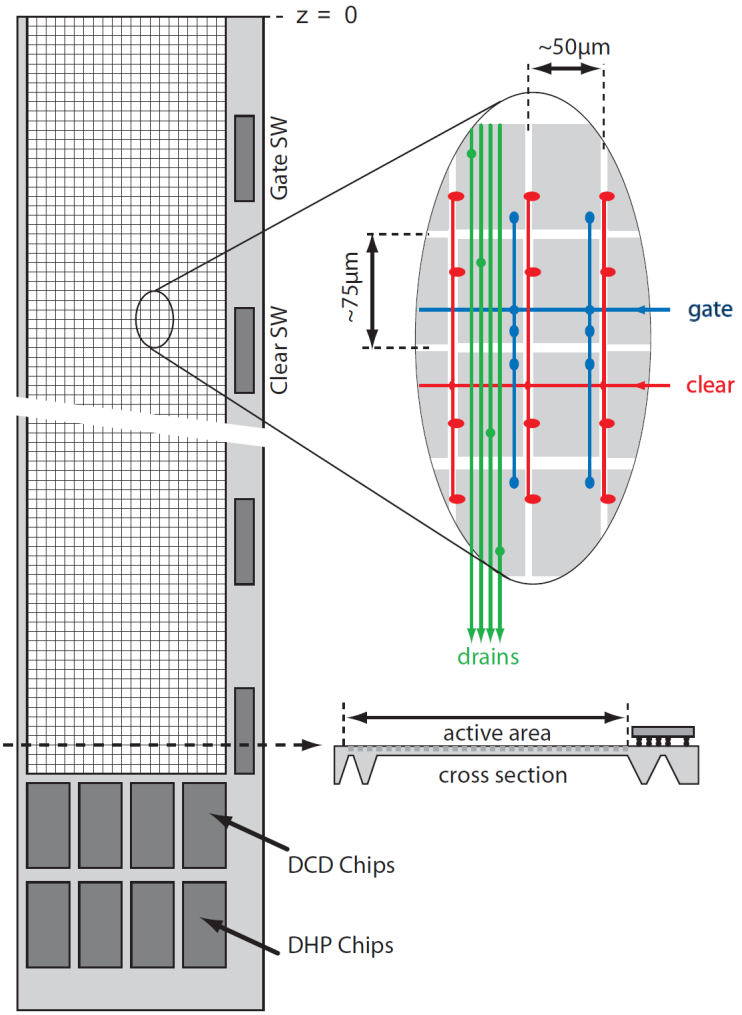

Figure 2.3: Readout geometry for DEPFET. Please notice you can see only half of the sensor [16].

The area of one DEPFET ladder contains 512 × 1600 pixels. Each DEPFET sensor is split into 2 parts, read by independent eletronic from opposite sides so actually we have 512 × 800 pixels. The readout consist of 3 kinds of ASICs[1] (see also figure 2.3). The SWITCHERs, which switch on the specific row to send current to DCDs, are placed along the side of DEPFET sensor on the rim. The DCDs (Drain Current Digitizer) which digitize currents from the row of pixels. The DHPs (Digital Handling Processor) buffer and analyze digital data streams and perform zero suppression [16]. Both DCDs and DHPs are placed at the ends of the sensor.

[1]Application-Specific Integrated Circuit

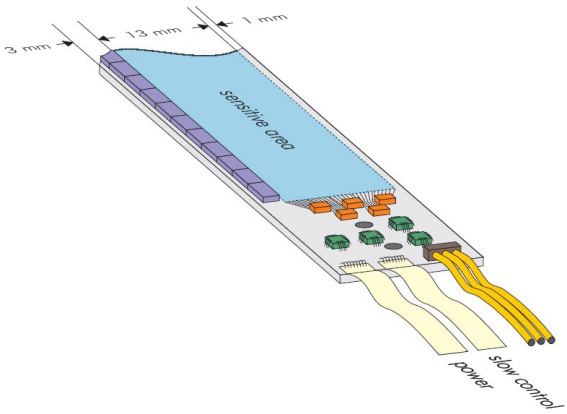

Figure 2.4: Illustrative picture of DEPFET sensor design.

The electronics, the electrical consumption cables, slow control, cooling systems are placed at both short sides of the ladder outside the sensitive volume of the vertex detector (Fig. 2.4). The power consumption of switcher chips will be very low (together around 1W), as only one row must be steered at a time. Similary for active area (again 1W). That is the reason, why we do not need special cooling in the active area. However, active cooling is expected for DCDs and DHPs area, because every DCD and DHP will consume 1W so we have together 8W. Whole vertex detector should consume in average about 360W [16].

2.4 Testbeams results

In spite of the fact that DEPFET can be thinned down to 50μm, the proposed DEPFET sensors for Belle II experiment will have thickness of 75μm. The reason is that Belle II experiment needs excellent spatial resolutions for tracking and vertexing due to their influence of the physics performance. The total spatial resolution of PXD and also SVD detectors is shown in figure 2.6. We can see better resolution for the 75μm DEPFET sensors.

Several testbeams have been performed in last years, namely 6 GeV electron beam at DESY (Deutsches Elektronen-Synchrotron), 24 GeV proton beam at CERN PS (Proton Synchrotron) and 120 GeV pion beam at CERN SPS (Super Proton Synchrotron). For the detailed descrition and analysis of various testbeams it is strongly recommended to have a look at some testbeam reports [17, 24, 23]. DEPFET setup modules used in these testbeams had pixel sizes in range from 20 $\times$ 20 μm^2 to 24 $\times$ 32 μm^2 , but Belle II sensors will have pixel sizes 50 $\times$ 50 μm^2

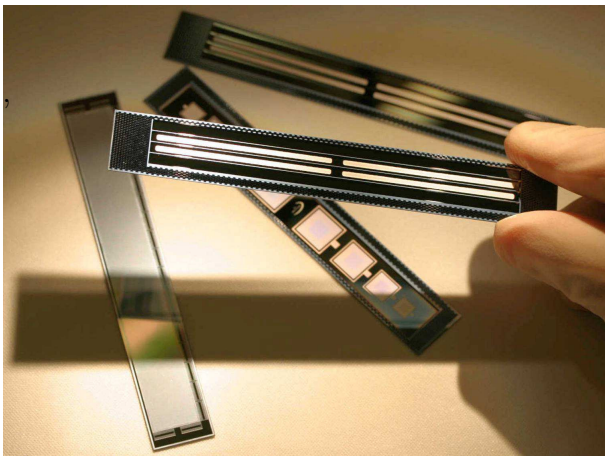

Figure 2.5: One of the first dummy DEPFET sensors.

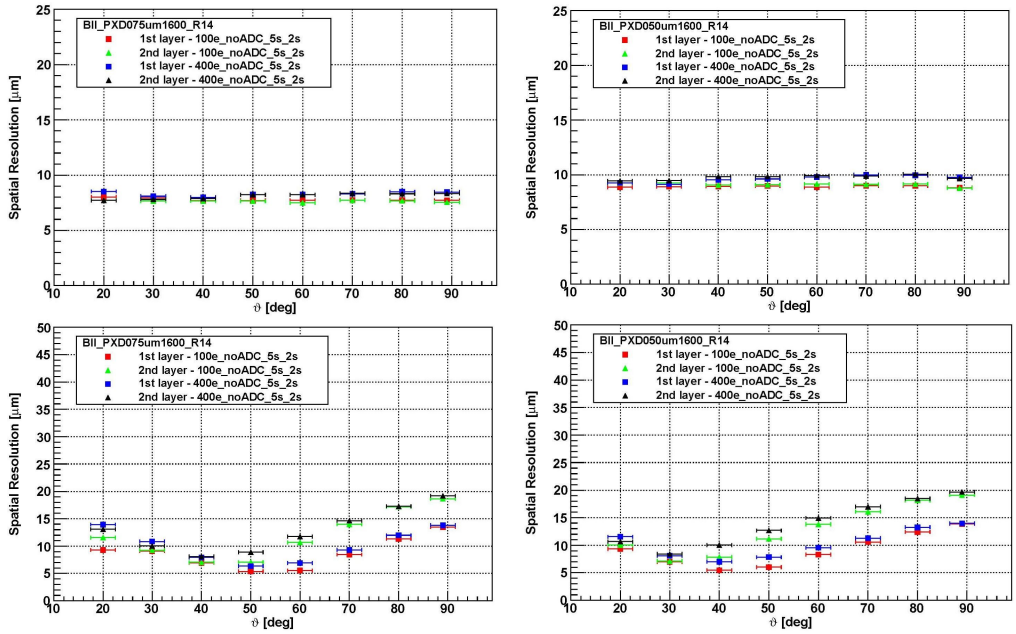

Figure 2.6: Spatial resolutions in R-ϕ (top) and Z (bottom) of 75μm (left) and 50 μm (right) DEPFET sensors [30].

and 75×50 μm^2. One of the most interesting results coming from testbeams is the spatial resolution of DEPFET, which is $\approx 1\mu$m with typical accuracy 0.1μm.

Another interesting results show that the internal amplification of the DEPFET g_q (gain of charge), which can be expressed by formula (I_d is drain current)

$$g_q = \frac{\Delta I_d}{e^-} \tag{2.1}$$

is aproximately equal 560 pA/e^-. All DEPFET modules used in testbeam were ILC types, but we learned how to handle analysis and also we tried overall manipulation with such a detector. First DEPFET-Belle II prototype testbeam is scheduled for year winter 2011.

Chapter 3

Basf2

As it has been already mentioned in chapter 2, Belle II will produce 50 times more data than Belle so the computing system has to be able to handle such an amount. It is expected to have 10^{10} events per year. On the other hand there also must be some computing power for physical analysis. It was decided that all Belle II members will provide that computer power. It basicly means that experiment will use grid computing model with the center at KEK.

3.1 Framework

Belle Analysis Framework (basf) will not be used anymore. The new framework called Belle 2 Analysis Framework (basf2) will be used instead. C++ and Python will be mainly used programming languages for offline software. The whole framework contains so called packages, which are actually containers for source code. Every package has its own librarian who is responsible for the code. There are also authors, who can be named by librarian and they can also contribute with writing code.

It was also decided that following systems will be supported [16]

1. Scientific Linux 5 [10]
2. CentOS [1]
3. Ubuntu [11]
4. MacOS [7]

Documentation is created with Doxygen tool [2] and official compiler is gcc-v4 [6]. There are nightly builds of framework which are not stable and bugs can appear. If the package is ready for using, librarian should tag it and these tagged packages can be included in the official release.

Typical data processing consist of so called module chain. Modules are small processing blocks with different tasks. Everything that happens in basf2 framework is done by these modules. If you put modules in some sophisticate way, so they are arranged in linear order, you will get set of modules which is called path. There can be, of course, more than one path in basf2. Figure 3.1 shows a possible

situation. The module chain starts with the module #1 and module #2. Let us stop here for a second. We said there could be more than one path in basf2, but now we see that these paths are connected through conditions. If the module #2 returns value greater than 5, framework will continue with path 2, otherwise path 1 would continue. The same situation is after condition of module #4. If the return value is true the framework will stop processing, in the other case it would switch to path 3 and continue with processing module #8.

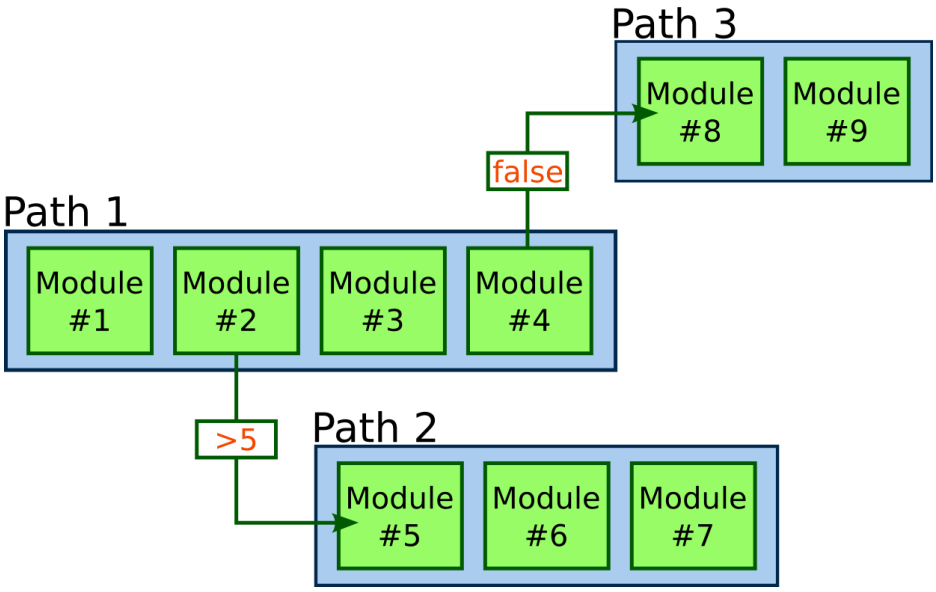

Figure 3.1: Modules chain and path illustration in basf2 [14].

3.2 Geometry

All of the detector parameters are stored centrally so every part of detector works with the same parameters. Geometry needed for full simulation and reconstruction is created from this central storage. Figure 3.2 shows this architecture.

Parameters in parameter storage are stored via XML documents [4]. These documents have hierarchical structure and you can easily include another XML document into existing one via XInclude technology [12].

Detector geometry is decribed by boxes, tubes, cones, and various geometry objects. These values are stored in XML documents. But how is the whole geometry built? That is job for C++ source code files. The geometry objects are implemented using ROOT TGeo objects, which are developed at CERN[1]. The scheme of this process is shown on the figure 3.2.

[1]In May 2011, it was decided to use the Geant4 [5] geometry instead.

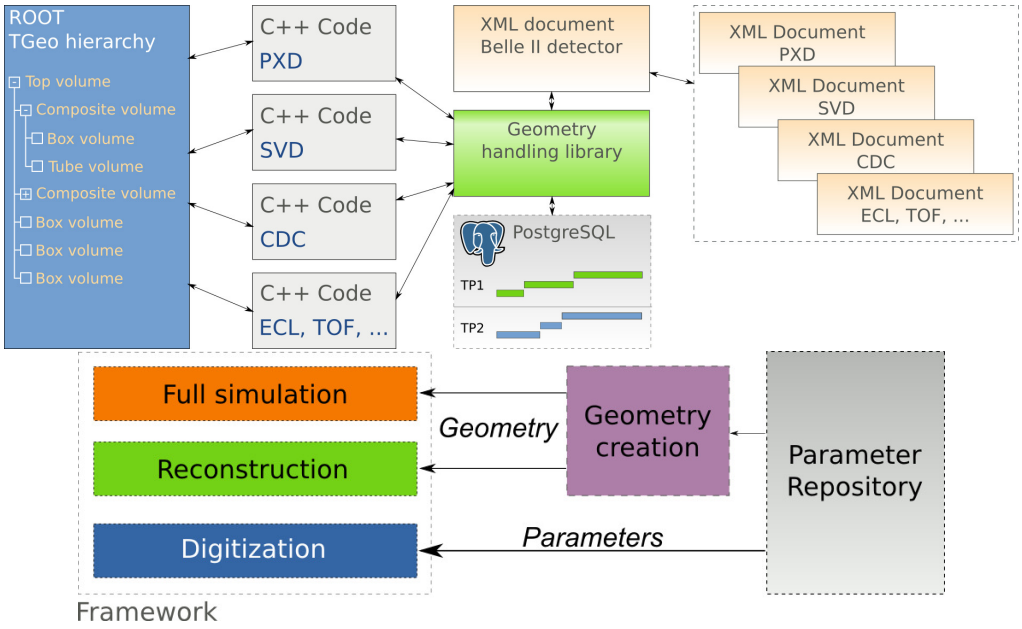

Figure 3.2: Geometry is created through C++ code from the centrally stored parameters. The digitization takes parameters from parametry repository. Said in other words, parameters store information about detector and C++ code creates geometry.

3.3 Simulation

The simulation normally consist of three parts

- event generation
- passage of particles through matter
- digitization

First part generates particles we would like to study (B mesons,...). This generation contains all information like production vertex, momentum, position, deposited energy, etc. B decays are generated by EvtGen [3], $e^+e^- \longrightarrow q\bar{q}$ events by Pythia [9] and EvtGen, τ-pair production by KKCM [37] and tauola [28].

Second part simulates interaction of particles which go through detector. The information about sensitive volumes is stored for later usage. Detector simulation is covered by Geant4 [5].

Last part of simulation process, digitization, can be described as response of detector components. We have to cover physics processes which take place in the detector, like electronic effects, signal generation and storage, creation of hits. The output we get is the same as in real situation and is represented by digits - detector signals.

Chapter 4

Energy losses in material

4.1 The Bethe-Bloch formula

The interactions of charged particles with speed $v = \beta c$ (c is speed of light in vacuum) leads to ionization or atomic excitation. The energy losses for the relativistic charged heavy particles are in agreement (we will talk about the exceptions later) with Bethe-Bloch formula [27]

$$-\left\langle \frac{dE}{dx} \right\rangle = Kz^2 \frac{Z}{A} \frac{1}{\beta^2} \left[\frac{1}{2} \ln \frac{2m_e c^2 \beta^2 \gamma^2 T_{max}}{I^2} - \beta^2 - \frac{\delta(\beta\gamma)}{2} \right] \tag{4.1}$$

which describes energy losses in the in the interval $0.1 < \beta\gamma < 1000$. If the $\beta\gamma$ factor is less than 0.1, velocity of incident particle is comparable to the velocities of electrons in atoms of absorber. On the other hand ($\beta\gamma > 1000$) radiative effects started to play important role.

Let us describe symbols used in Bethe-Bloch formula. We will start with constant K

$$K = 4\pi N_A r_e^2 m_e c^2 = 0.307\ 075 \text{ MeV cm}^2 \text{ mol} \tag{4.2}$$

where $N_A = 6.022 \times 10^{23}$ mol^{-1} is Avogadro number, $r_e = 2.817$ fm is classical electron radius and $m_e c^2 = 0.511$ MeV is electron mass multiplied by factor c^2. Other symbols in Bethe-Bloch formula (4.1) have following meaning:

- z - Charge of incident particle
- Z - Atomic number of absorber
- A - Atomic mass of absorber
- $\gamma = \dfrac{1}{\sqrt{1-\beta^2}}$ - Gamma factor
- I - Mean excitation energy
- $\delta(\beta\gamma)$ - Density effect correction to ionization energy loss (see following chapter)
- T_{max} - Maximum kinetic energy which can be transfered to free electron of absorber in a single collision

T_{max} is given by formula

$$T_{max} = \frac{2m_e c^2 \beta^2 \gamma^2}{1 + 2\gamma \frac{m_e}{M} + \left(\frac{m_e}{M}\right)^2} \tag{4.3}$$

where M is mass of incident particle. Note that you can simplify this formula to

$$T_{max} = 2m_e c^2 \beta^2 \gamma^2 \tag{4.4}$$

in the case that $2\gamma m_e \ll M$.

4.2 Density effect

Every charged particle passing through absorber inclines to polarize absorber's atoms. Therefore, electrons far away from the path of the particle do not interact so much with it, so we see some decrease in energy loss calculated by Bethe-Bloch formula. This effect depends on the energy of the charged particle and on the density of absorber (therefore the name *density effect*).

According to Shernheimer [39] density effect correction $\delta(\beta\gamma)$ can be calculated by formulas

$$\delta(\beta\gamma) = 2(\ln 10)X + a(X_1 - X)^m + C \ , \qquad X_0 < X < X_1 \tag{4.5}$$

$$\delta(\beta\gamma) = 2(\ln 10)X + C \ , \qquad X > X_1 \tag{4.6}$$

X is variable introduced by Sternheimer

$$X = \log_{10}\left(\frac{p}{mc}\right) = \log_{10}(\beta\gamma) \tag{4.7}$$

All other parametres (a, m, X_0, X_1, C) depend on material. In Sternheimer paper [36] you can find most of the common used materials and compounds. Sternheimer also provided formula for C as

$$C = -2\ln\left(\frac{I}{\hbar\omega_p}\right) - 1 \tag{4.8}$$

$\hbar\omega$ is often called plasma energy and can be calculated as [27]

$$\hbar\omega = \sqrt{\rho\frac{Z}{A}} \times 28.816 \text{ eV} \tag{4.9}$$

As an example, pay attention to figure 4.2 where you can see energy losses with and without density effect correction.

4.3 Fluctuactions

Until now we have talked mainly about *mean* energy loss of charged particle passing through absorber. But this value is not equal to the experimetal data.

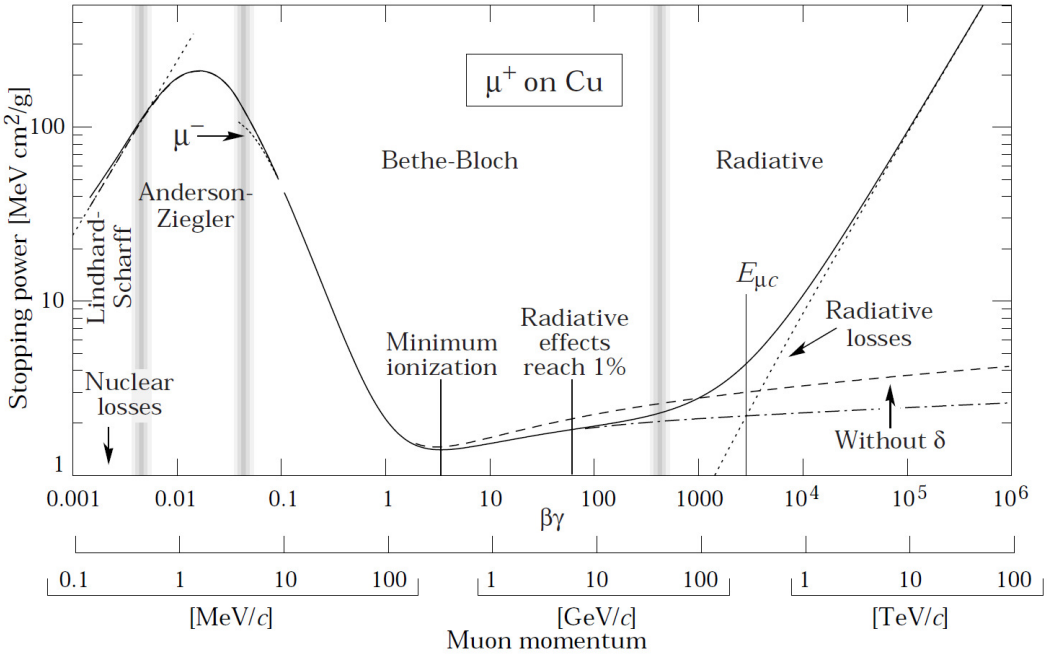

Figure 4.1: Energy loss of the mion in the copper as the function of $\beta\gamma$ [27].

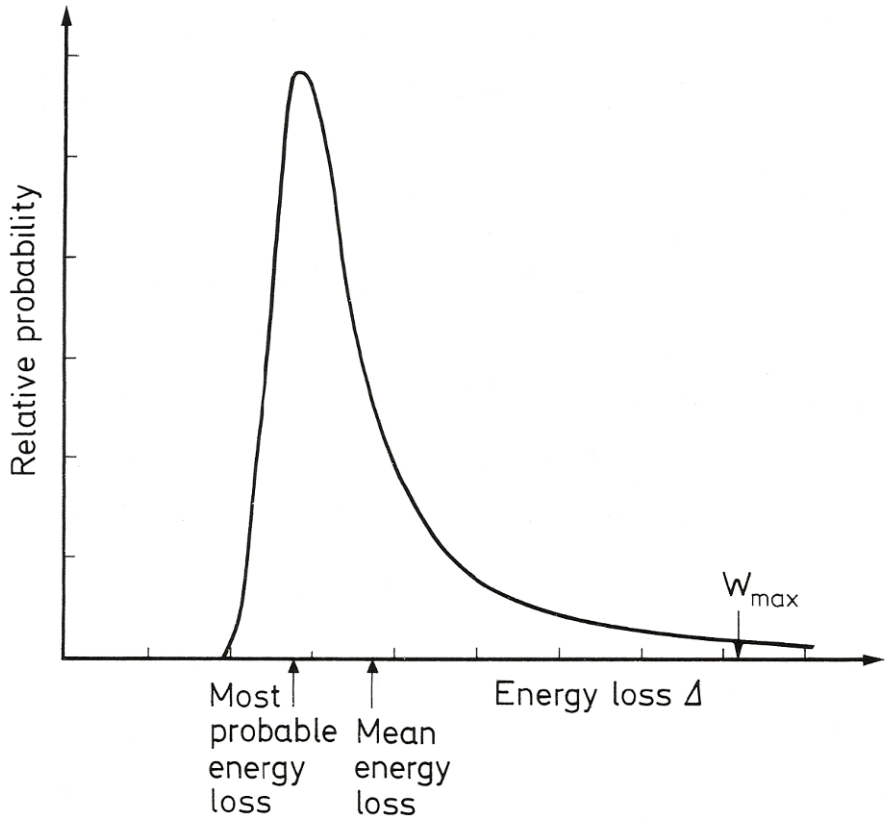

Figure 4.2: Distribution in energy loss and difference between most probable value and mean value of energy loss [32]. W_{max} is in this theis equal to T_{max}.

For instance, if we have the monoenergetic beam passing through absorber, we would rather see some distribution in energy than a delta function (figure 4.2). Generaly, it is quite difficult to calculate the distribution in energy losses for absorber of given thickness. However, two soviet physicists, Landau and Vanilov, tried to solve this problem.

The result of their work is that the energy loss probability distribution is described by Landau-Vavilov distribution [31, 40] . The most probable energy loss is [13]

$$\Delta_p = \xi \left[\ln \frac{2mc^2\beta^2\gamma^2}{I} + \ln \frac{\xi}{I} + j - \beta^2 - \delta(\beta\gamma) \right] \tag{4.10}$$

where $j = 0.200$ and

$$\xi = \frac{xKZ}{2A\beta^2} \tag{4.11}$$

for a absorber of thickness x in g cm^{-2}. The density correction $\delta(\beta\gamma)$ was later included to the formula 4.10 by Bichsel [13]. In figure 4.3 we can see the difference between Bethe-Bloch $\frac{dE}{dx}$ and Landau-Vavilov-Bichsel $\frac{\Delta_p}{x}$ in silicon absorber as a function of muon energy.

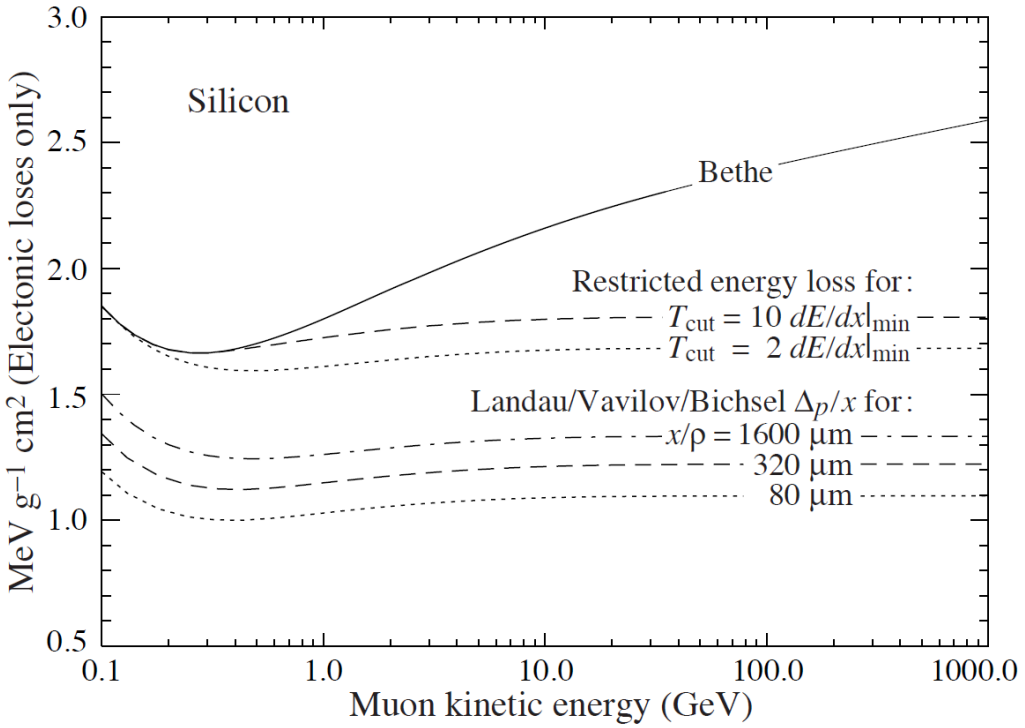

Figure 4.3: Differences between Bethe-Bloch energy loss, restricted energy loss and Landau-Vavilov-Bichsel most probable value of energy loss per unit thickness in silicon absorber.

The Landau-Vavilov-Bichsel theory was confronted with experiments made by Bak in 1982. The experiments were done on silicon and germanium detectors of various thickness (32, 51, 100, 174, 290 and 1040 μm). The most important results are shown in the figures 4.4 and 4.5. Measured particles were protons, pions and electrons (from top to bottom), the dashed line represents theoretical function for energy loss, solid line represents Bak's theory and circles represents values obtained from experiment. It can be clearly seen that Landau-Vavilov-Bichsel theoretical value of most probable energy loss is in very good agreement with experiment for higher values of thickness (1040μm, 290 μm, 100μm). On the other hand, we can see small differences for 51μm thin silicon detector.

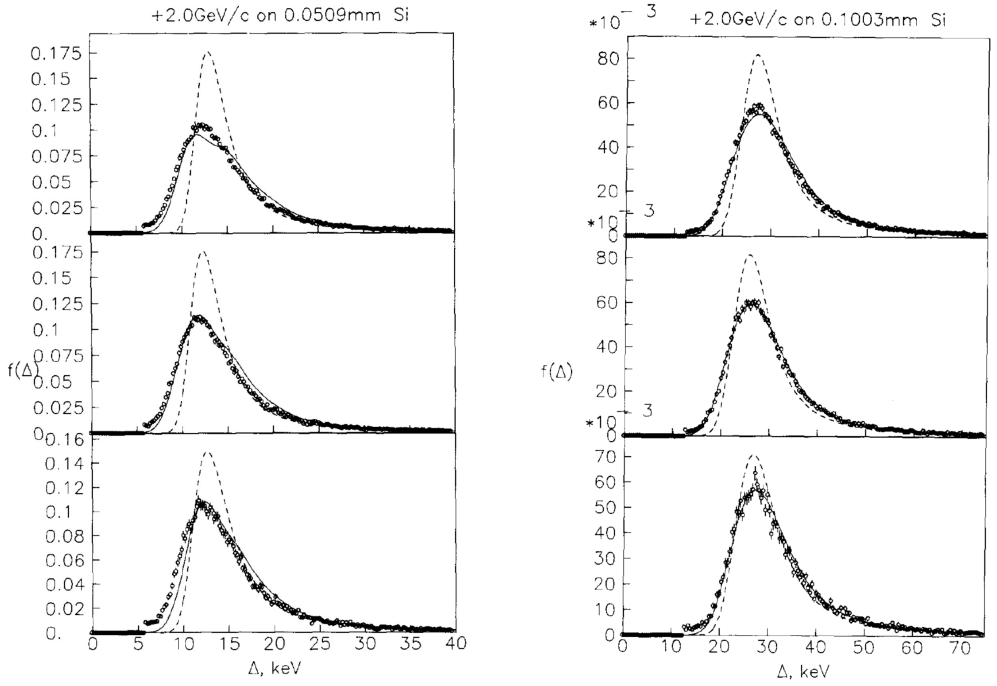

Figure 4.4: Energy loss distributions for 51μm (left) and 100μm (right) silicon. Dashed line is Landau function and the dots are results from the experiment. The upper distribution is for 2GeV/c positrons, middle for 2GeV/c pions and the lower for 2GeV/c protons.

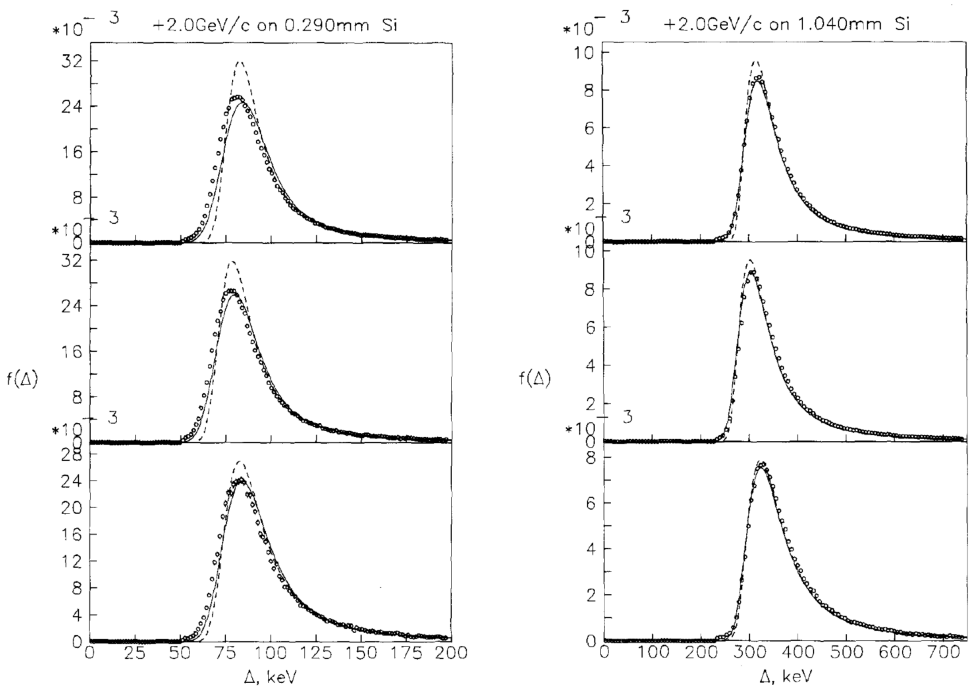

Figure 4.5: The same as for figure 4.4 but for 290μm (left) and 1040μm (right) thin silicon.

4.4 Mixtures and compounds

If we have mixture or compound, we can say it is made of layers in right proportion. These layers are of course made of pure material. Energy loss is then given as:

$$\frac{dE}{dx} = \sum_j w_j \left.\frac{dE}{dx}\right|_j \tag{4.12}$$

Here $\left.\frac{dE}{dx}\right|_j$ is the mean rate of energy loss in the j-th element.

However, equation 4.12 cannot be used for obtaining $\langle I \rangle$, because electrons in compounds or mixtures are strongly bounded. Therefore, it is better to calculate it as follows [38]. Let us take for example molecule of CH_4. There are 6 electrons of carbon atom, 4 electrons of hydrogen atoms, together 10 electrons in the molecule. The total mean excitation energy of CH_4 is then

$$\ln I_{CH_4} = \frac{6}{10} \ln I_C + \frac{4}{10} I_H \tag{4.13}$$

where I_C is mean excitation energy of carbon and I_H is mean excitation energy of hydrogen.

4.5 Geant4 calculation of energy loss fluctuactions

The Geant4 framework [5] uses very simple model of energy fluctuactions in thin absorbers. This model is based on atoms, which have only 2 energy levels E_1 and E_2. The interaction between particle and atom can be either ionization or excitation to energy level E_1 or E_2. Energy loss by ionization is distributed according to $g(E)$ function as [8]:

$$\int_{E_0}^{T_{up}} g(E)dE = 1 \Longrightarrow g(E) = \frac{E_0 T_u p}{T_u p - E_0}\frac{1}{E^2} \tag{4.14}$$

E_0 is ionization energy and T_{up} is energy treshold for δ-electrons production. The macroscopic cross section for ionization is

$$\Sigma_{ion} = C\frac{T_{up} - E_0}{T_{up}E_0 \ln\dfrac{T_{up}}{E_0}}r \tag{4.15}$$

where C and r are model parameters. On the other hand the macroscopic cross section for excitation is defined as

$$\Sigma_{ex} = C\frac{f_i}{E_i}\frac{\ln\left(\dfrac{2mc^2(\beta\gamma)^2}{E_i}\right) - \beta^2}{\ln\left(\dfrac{2mc^2(\beta\gamma)^2}{I}\right) - \beta^2}(1-r) \tag{4.16}$$

E_i is energy level and f_i corresponding oscillator strength. These parameters have been chosen as:

$$f_2 = 0, \quad Z = 1 \tag{4.17}$$
$$f_2 = 2/Z, \quad Z \geq 2 \tag{4.18}$$
$$E_0 = 10\text{eV} \tag{4.19}$$
$$E_2 = Z^2 \times 10\text{eV} \tag{4.20}$$

Parameters f_1 and E_1 can be calculated from formulas

$$f_1 + f_2 = 1 \tag{4.21}$$
$$f_1 \ln E_1 + f_2 \ln E_2 = \ln I \tag{4.22}$$

It can be shown [8] that

$$C = \frac{dE}{dx} \tag{4.23}$$

so now we have only one parameter which can be changed, r. It was decided to fix this parameter as

$$r = 0.55 \tag{4.24}$$

Chapter 5

Simulation

Let me finally use all information described in previous chapters and compare achieved results. The simulation for PXD sensor and also for SVD one was made. Following sections show results and describe them.

5.1 Verification of Bichsel-Landau-Vavilov formula

First of all, a simple geometry which consist of silicon layer of specific thickness surrounded with the detector was created. The thicknesses were the same as Bichsel used in his paper [13]. During the estimation of energy loss, the question was how to get this value from simulation. Finally it was decided to use this idea. The basf2 framework (or better said, Geant4) provides information of the particle momentum at any time. As you can choose type of particle and its momentum at the beginning p_i through particle gun script, it is simple to calculate the energy loss of the particle from relativistic formula

$$\Delta E = E_i - E_f = \sqrt{m^2c^4 + p_i^2c^2} - \sqrt{m^2c^4 + p_f^2c^2} \tag{5.1}$$

where E_i and E_f are energies of particle at the beginning and the end, p_f final momentum, m is rest mass of particle.

Figure 5.1 shows the results for 174μm and 100μm thick silicon. The pions with energies 2GeV were used. It can be clearly seen that both energy distributions have the same shape, which is similar to Landau function, but it is not. The most probable value of energy loss is close to 47 keV and 26 keV respectively.

To see and compare results, all values that characterize energy loss in thin absorbers were put into table 5.1. There you can see values of the most probable energy losses Δ_p and full width at half maximum w calculated by Bichsel [13]. Then you can find there values gotten from simulation and calculation from momentum method (see formula 5.1). These table shows that Δ_p simulation values are in agreement with theoretical values. There is little difference in w as thickness becomes greater which is sign that 2 level model used by Geant4 does not perfectly describe straggling functions.

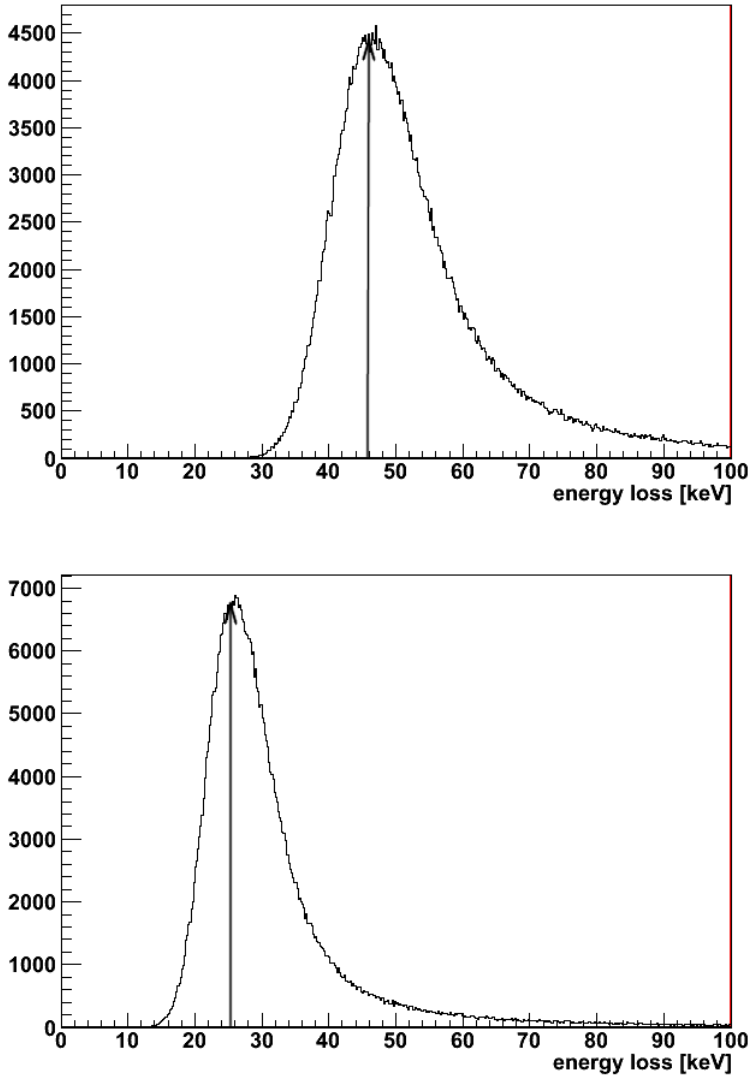

Figure 5.1: Energy loss distribution in 174μm (up) and 100μm (down) thick silicon. Both have the similar and expected shape. Arrows in the pictures show theoretical values of the most probable energy loss.

Table 5.1: Comparison of energy losses parameters (Δ_p and w) calculated by Bichsel [13] with results gotten from simulation.

	Bichsel's results		results from simulation	
thickness [μm]	Δ_p [keV]	w [keV]	Δ_p [keV]	w [keV]
1040	302.3	84.18	303 ± 1.5	80 ± 3.0
290	78.49	28.87	78.5 ± 1.5	26 ± 2.0
174	45.92	20.50	46.1 ± 1.0	17 ± 1.5
100	25.28	12.93	25.5 ± 1.0	11.5 ± 1.5
51	11.84	7.20	12.3 ± 0.6	7.5 ± 1.0
32	7.092	5.17	7.3 ± 0.3	5.2 ± 0.5

5.2 Verification of Bethe-Bloch formula

Until now, it has been understood that we always work with thin silicon detectors. All Bichsel theory is valid, but only for silicon. If we would like to describe energy losses in other materials, we cannot simply compute most probable value Δ_p or full width at half maximum w. But we can still use Bethe-Bloch formula and compare it with simulation values.

First let us compare Bethe-Bloch formula and simulation results for thin silicon, even if there is much better theory for it. There was used the same data, but now the mean values were watched.

The mean value for low thicknesses is highly influenced by "tail" of distribution function. Even one value from the "end" of the tail can significantly increase the mean value. It is clearly seen the mean value is very distorting indicator. To prevent this situation to happen, we apply the concept often used with normal distribution called three-sigma rule. This rule says almost all values (99.73%) lie within 3 standard deviations of the mean for the normal distribution. For the energy loss distribution it simply means the last 0.27% of the data were cut off.

Table 5.2: Comparison of mean energy loss values calculated by Bethe-Bloch formula and energy loss values from simulation.

thickness [μm]	Bethe-Bloch [keV]	Simulation [keV]
1040	468.3	464.2
290	130.6	132.7
174	78.35	79.24
100	45.03	47.53
51	22.96	24.36
32	14.41	15.92

5.3 Results for PXD

Inner pixel detector is mostly made of silicon (see table 5.3). There is also gold used but total fraction of this PXD material is less than 0.1%. From the previous section we know that for silicon we have pretty good theory of energy losses. The most probable energy loss value is described by Landau-Vavilov-Bichsel formula 4.10.

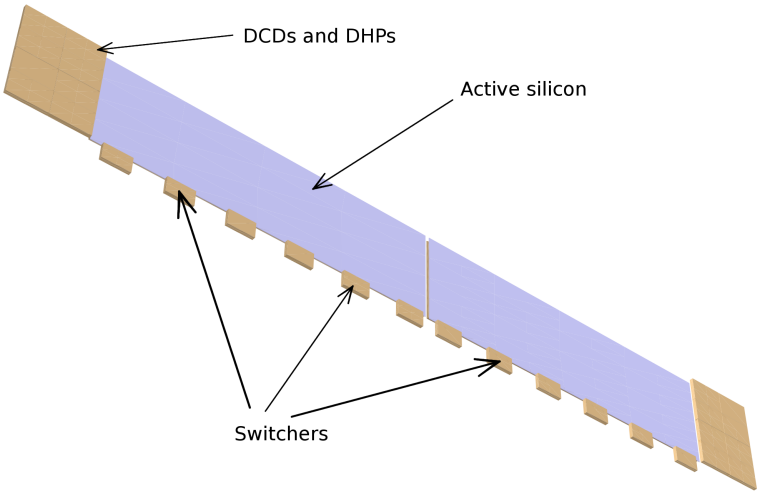

Figure 5.2: Testing geometry for PXD. Please notice you cannot see the rim of the detector which is also called passive silicon.

First, let us have a look at the PXD geometry. Looking at the figure 5.2 you can see two sensors which make one ladder. The blue part is active silicon, small boxes at the left and right side are DCDs and DHPs, in the bottom, there are Switchers. You cannot see the silicon rim, which is often called passive silicon, on which the chips and sensitive silicon are placed.

Table 5.3: Materials used in the PXD geometry. The passive silicon density is due to material reduction expected to decrease its value to one third.

compound	material	density [g cm^{-3}]	fraction
active	silicon	2.33	1.0000
passive	silicon	2.33	1.0000
Switcher	silicon	2.41	0.9956
	gold	19.3	0.0044
DHP	silicon	2.49	0.9908
	gold	19.3	0.0092
DCD	silicon	2.49	0.9908
	gold	19.3	0.0092

In the simulation the same procedure was used as in the previous section. First the particle gun was moved along whole area of one PXD ladder (so called uniform distibution). The particles were shot perpendicular to the plain in which PXD lied. You can see three possible situations which can happen in the picture 5.3. The first possibility 1.) corresponds to the situation when the particle cross only the active silicon of the sensor. Second situation 2.) describes particles which travel throught rim or passive silicon. The last option 3.) is generated by particles which enter the passive silicon and leave the sensor at the place where chips are (DCDs, DHPs or Switchers).

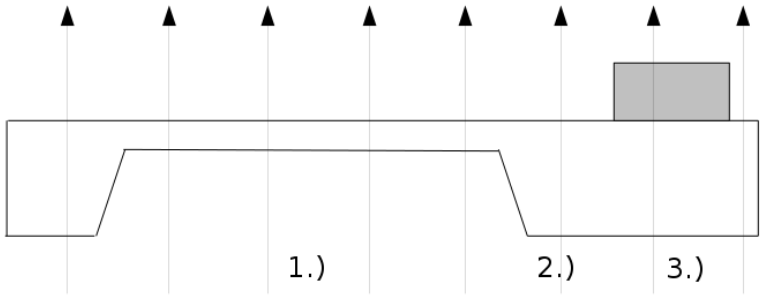

Figure 5.3: Charged particle travelling perpendiculary to the PXD sensor can cross it at 1.) the active part (75μm), 2.) passive part (420μm) or 3.) passive+chips part (920μm).

Again, all values were put into the table 5.3. The results are in very good agreement with theory in spite of the fact there are minor non-silicon materials in the pixel detector. But their ratio is very small.

Table 5.4: Energy losses in PXD, theoretical values and simulation.

	theory [13]		simulation	
position	Δ_p [keV]	w [keV]	Δ_p [keV]	w [keV]
1.) active	18.2	10.27	18.5 $\pm$ 0.6	9.5 $\pm$ 1.0
2.) passive	114.8	39.35	115.5 $\pm$ 1.5	35 $\pm$ 2.0
3.) chips	264.5	76.60	265.0 $\pm$ 1.5	72 $\pm$ 3.0

5.4 Results for SVD

Geometry of SVD is different from the PXD geometry (see table 5.5). There are 4 layers and ladders in layers are composed of 4 different kinds of sensors. See figure 5.4 for better understanding. Under the sensors there are carbon ribs, on some of sensors there is electronic (chips) and above sensors there is cooling pipe (see figure 5.5).

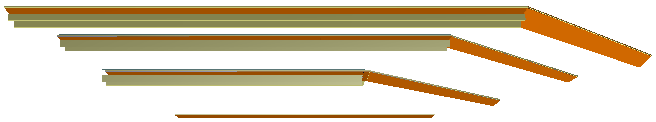

Figure 5.4: Testing geometry for the SVD.

Simulation was done again in the way as before. Particle gun was shot to various places of the SVD layers. To be more specific, through basic sensor (1.) - compound of silicon, rohacell and kapton), then through basic sensor and chips (made of silicon) (2.), the last option was through basic sensor, chips and also cooling pipe (steel and CO_2 - liquid) (3.) as it is explained in figure 5.5. Because of the fact the SVD consists of layers which are not made only of silicon, it was decided to use Bethe-Bloch formula as was discussed in section 5.2. Results are once again summarized in table 5.6.

Table 5.5: Materials used in the SVD geometry.

compound	material	density [g cm^{-3}]	fraction
basic sensor	silicon	2.330	0.1875
	rohacell	0.032	0.6250
	kapton	1.530	0.1875
chips	silicon	2.330	1.0000
cooling pipe	steel	8.000	0.0667
	carbon dioxide	0.042	0.9333

Table 5.6: Energy losses in SVD, theoretical values and simulation.

position	Bethe-Bloch [keV]	simulation [keV]
1.) basic sensor	177	179
2.) sensor + chips	359	363
3.) sensor + chips + cooling pipe	385	403

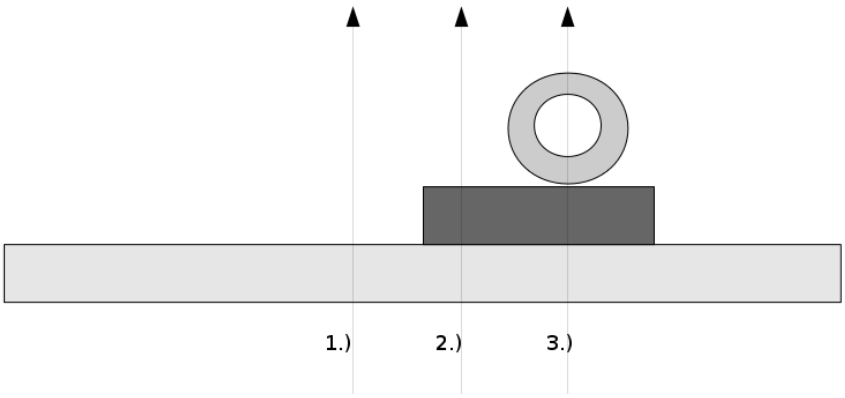

Figure 5.5: Particle gun shooting into 3 different places of SVD sensor.

5.5 Discussion

For verification of thin silicon materials, the Landau-Vavilov-Bichsel formula was used. The variables describing energy loss in thin silicon, Δ_p and w are in agreement with theory. The distributions have expected shape, which is close to Landau's function.

For non-silicon materials, it was decided to stay with Bethe-Bloch formula, due to lack of the theory for non-silicon thin materials. Bethe-Bloch's variable describing energy loss is mean value of the energy loss $\frac{dE}{dx}$.

The PXD and SVD geometry was created and the energy losses at various places of the detectors were measured and compared with theoretical values. As the PXD is whole made almost from silicon the theoretical values and simulation are in perfect agreement.

The SVD consist of more materials and the simulation and theoretical mean values are also in good agreement, but the mean value is not appropriate parameter, due to assymetric distribution of energy losses. It was showed this parameter is not proper and the simulation values which are from the end of the tail of the distribution (high energy values) can significantly influence the total mean value of $\frac{dE}{dx}$ (increase of the mean value).

Conlusion

The theory of energy loss of the charged particle has benn studied. More effort was spent to understand the energy loss in thin silicon absorbers, because nowadays various silicon detectors are heavily used in many particle physics experiments. The geant4's 2 level model of energy loss has also been studied.

To validate the energy loss in PXD and SVD of the Belle II detector, the basf2 framework needed to be understood. It has also been required to change the geometry, write some scripts and analyse the data from simulation. All theoretical knowledge has been put together and compared with the simulation.

This work has also contained check and correctness of material implementation into basf2. Severals mistakes or misunderstandings have been found, discussed with PXD or SVD experts and corrected. For future planned changes in inner detector geometry it will be essential to do this check due to preventing of trivial errors in material budget. These errors may have serious unwanted consequences.

Bibliography

[1] Centos, http://www.centos.org/.

[2] Doxygen, http://www.doxygen.org.

[3] Evtgen, http://www.slac.stanford.edu/ lange/evtgen/.

[4] Extensible markup language (xml), http://www.w3.org/xml/.

[5] Geant4, http://geant4.web.cern.ch/geant4.

[6] GNU compiler collection, http://gcc.gnu.org/.

[7] Macos, http://www.apple.com/macosx/.

[8] Physics reference manual for geant4 9.4, 17 December, 2010, http://geant4.web.cern.ch/geant4/userdocumentation/usersguides/ (available online 2 August, 2011).

[9] Pythia, http://home.thep.lu.se/ torbjorn/pythia.html.

[10] Scientific linux, http://www.scientificlinux.org/.

[11] Ubuntu, http://www.ubuntu.com/.

[12] Xinclude, http://www.w3.org/tr/xinclude/.

[13] H. Bichsel. Straggling in thin silicon detectors. *Rev. Mod. Phys.*, 60:663, 1988.

[14] Private communication with Andreas Moll.

[15] Private communication with Zděnek Doležal.

[16] Z. Doležal and S. Uno et al. Belle II technical design report. 2010.

[17] J. J. Velthuis et al. A DEPFET based beam telescope with submicron precision capability. *IEEE TNS*, 55:662, 2008.

[18] K. Abe et al. Belle. *Phys. Rev.*, D66: 032007 (2002), hep–ex/0202027, 10.1103/PhysRevD.66.032007.

[19] K. Abe et al. Belle. *Phys. Rev.*, D68: 012001 (2003), hep–ex/0301032, 10.1103/PhysRevD.68.012001.

[20] K. Abe et al. Belle. *Phys. Rev. Lett.*, 93: 021601 (2004), hep–ex/0401029, 10.1103/PhysRevLett.93.021601.

[21] K. Abe et al. Belle. *Phys. Rev. Lett.*, 93: 191802 (2004), hep–ex/0408100, 10.1103/PhysRevLett.93.191802.

[22] K. Ikado et al. Belle. *Phys. Rev. Lett.*, 97: 251802 (2006), hep–ex/0604018, 10.1103/PhysRevLett.97.251802.

[23] L. Andricek et al. Intrinsic resolutions of DEPFET detector prototypes measured at beam tests. *Nucl. Instrum. Meth. A*, 638:24, 2011.

[24] P. Kodys et al. Spatial resolution analysis of micron resolution silicon pixel detectors based on beam and laser tests. *Nucl. Instrum. Meth. A*, 604:385, 2009.

[25] S. K. Choi et al. Belle. *Phys. Rev. Lett.*, 91: 262001 (2003), hep–ex/0309032, 10.1103/PhysRevLett.93.262001.

[26] S.-W. Lin et al. Belle. *Nature*, 452: 332 (2008), 10.1038/nature06827.

[27] K. Nakamura et al. (Particle Data Group). 2010 review of particle physics. *J. Phys. G*, 37, 075021 (2010).

[28] S. Jadach and Z. Was. *Comp. Phys. Commun*, 85:453, 1995.

[29] J. Kemmer and G. Lutz. *Nucl. Instrum. Meth. A*, 253:356, 1987.

[30] P. Kodys. The DEPFET active pixels - high resolution sensor for Belle II. ANIMMA conference talk, Ghent 2011.

[31] L.D. Landau. *J. Exp. Phys. (USSR)*, 8:201, 1944.

[32] W.R. Leo. *Techniques for nuclear and particle physics experiment.* 1994.

[33] Luminosity of KEKB. http://www-kekb.kek.jp/history/lumupdate.gif. available online 25.4.2011.

[34] P. Raimondi. 2nd SuperB workshop talk. 2006.

[35] KEK Press Release. KEKB/belle integrated luminosity reached 1000 fb^{-1}. Dec 8, 2009.

[36] M.J. Berger R.M. Sternheimer, S.M. Seltzer. The density effect for the ionization loss of charged particles in various substances. *Atomic Data and nuclear data tables*, 30:261, 1984.

[37] B. F. L. Ward S. Jadach and Z. Was. *Comp. Phys. Commun*, 130:360, 2000.

[38] M.J. Berger S.M. Seltzer. *Int. J. of Applied Rad*, 33:1189, 1982.

[39] R.M. Sternheimer. The density effect for the ionization loss in various materials. *Phys. Rev.*, 88:851, 1952.

[40] P.V. Vavilov. *Sov. Phys. JTEP*, 5:749, 1957.